Calibration of shell $\delta^{18}O$ from the common whelk *Buccinum undatum* highlights potential for palaeoenvironmental reconstruction

Philip R. Hollyman[1,2*], Melanie J. Leng[3,4], Simon R. N. Chenery[5], Hilary J. Sloane[3], Christopher A. Richardson[2].

1) British Antarctic Survey, High Cross, Madingley Road, Cambridge, CB3 0ET, UK
2) School of Ocean Sciences, College of College of Environmental Sciences and Engineering, Bangor University, Menai Bridge, Anglesey, LL59 5AB, UK
3) National Environmental Isotope Facility, British Geological Survey, Nottingham NG12 5GG, UK
4) School of Biosciences, University of Nottingham, Sutton Bonington Campus, Leicestershire LE12 5RD, UK
5) Centre for Environmental Geochemistry, British Geological Survey, Nottingham, NG12 5GG, UK

Corresponding Author email: Philip R Hollyman (phyman@bas.ac.uk)

Co-author emails: Melanie J. Leng (mjl@bgs.ac.uk), Simon R. N. Chenery (srch@bgs.ac.uk), Hilary J. Sloane (hjs@nigl.nerc.ac.uk), Christopher A. Richardson (c.a.richardson@bangor.ac.uk)

Abstract

The common whelk, *Buccinum undatum*, is a commercially important gastropod found throughout the North Atlantic. One method of age and life history analysis for gastropod species is the use of oxygen isotope ratio ($\delta^{18}O$) measurements from their shells, which is a well-established technique for the reconstruction of historical seawater temperatures at the time of shell biomineralization. Palaeotemperature calibrations have been developed for different types of calcium carbonate as well as species-specific equations to produce the most accurate seawater temperature reconstructions. Here we investigate the four-layer internal structure of *B. undatum* shells and confirm an aragonite composition using Micro-Raman Spectroscopy (MRS). We then calibrate a species-specific palaeotemperature equation for this gastropod species. This was achieved through the isotopic analysis of shells from laboratory reared specimens of known provenance reared at specific seawater temperatures to produce the following:

$$t(^{o}C) = 14.96 (\pm 0.15) - 4.94 (\pm 0.22) \times (\delta^{18}O_{shell} - \delta^{18}O_{water})$$

The calibrated equation differs significantly from previously published data derived from both aragonite and calcite. An offset of 1.04 ‰ (± 0.41 ‰) was discovered between observed $\delta^{18}O_{Shell}$ values and those expected under equilibrium, suggesting a species-specific vital effect. The calibrated equation was used to reconstruct accurate, high resolution historical seawater temperatures from three sites across the U.K. (Shetland, the Menai Strait and Jersey). With this new accurate calibration, both modern and fossil *B. undatum* shells now have the potential to be employed as high-resolution archives of recent and historical seawater temperature.

Keywords: Palaeotemperature; Oxygen Isotopes; Mollusc shells; Micro-Raman spectroscopy; vital effect

1. Introduction

There are many ways to reconstruct life and environmental histories using hard parts of molluscan species such as statoliths (squid−Arkhipkin, 2019; gastropods − Hollyman *et al*., 2018b), opercula (gastropods - Vasconlecos *et al*., 2012; Bökenhans *et al*., 2016) and beaks (cephalopods - Schwarz *et al*., 2019). However, the molluscan shell is the most regularly utilised and most reliable tool for historical reconstructions using palaeontological and modern specimens (e.g. Latal *et al*., 2004; Prendergast *et al*., 2013; 2015 and Steinheart *et al*., 2016 for review). Mollusc shells contain a plethora of information in the form of growth lines (allowing accurate age determination, Richardson, 2001) and shell chemistry, analysis of which can often result in proxies for environmental conditions at the time of mineralisation (Gillikin, 2005).

The use of oxygen isotope composition (expressed as $\delta^{18}O$) of mollusc shells as a proxy enabling reconstruction of past temperature (also known as palaeothermometry or stable isotope thermometry) is a widely used technique in the field of sclerochronology, for both bivalve and gastropod shells (see review: Leng and Lewis, 2016) and in molluscan palaeontology and palaeoecology (Latal *et al*., 2004). The seawater temperature at the time of formation can be retrospectively calculated using palaeotemperature equations that utilize both the $\delta^{18}O$ values of the shell calcium carbonate ($\delta^{18}O_S$) and the $\delta^{18}O$ values of the seawater ($\delta^{18}O_w$). Epstein *et al*. (1953), calibrated one of the first equations using a mix of aragonitic and calcitic marine shells over a wide range of temperatures. Since this seminal study, palaeotemperature equations have been calculated for different minerals (e.g. calcite [Kim and O'Neil, 1997, Leng and Marshall, 2004, Wanamaker *et al*., 2006]; aragonite [Grossman and Ku., 1986, Kim *et al*., 2007]) and types of organisms (e.g. various marine fish species [Patterson *et al*., 1993], corraline sponge [Böhm *et al*., 2000], bivalves e.g. *Mytilus edulis* [Wanamaker *et al*., 2006], gastropods e.g. *Conus ermenius* [Gentry *et al*., 2008]). It is now widely accepted that species-specific palaeotemperature equations should be calibrated to ensure the most accurate seawater temperature reconstructions (Bemis *et al*., 2002; Wejnert *et al*., 2013), due to perturbation by vital effects.

The term 'vital effect' refers to observed discrepancies between the composition of a biogenic carbonate and inorganic precipitation (Langer *et al*., 2020), with observed isotopic values differing from those expected if the carbonate was formed under isotopic equilibrium with the surrounding seawater. There are two general categories of vital effect; kinetic and taxonomic (Weiner and Dove, 2003). Kinetic effects appear to be most prevalent when an

organism is calcifying rapidly, resulting in isotopic disequilibrium from the surrounding water mass (e.g. McConnaughey 1989a; Weiner and Dove, 2003; Ziveri et al. 2003). Taxonomic effects are described when organisms exert biological control over the isotopic composition of their structures (Urey et al., 1951; Craig, 1953), resulting in clear disequilibrium from the surrounding water mass. However, isotopic records may still reflect environmental conditions (e.g. Flores *et al*., 2018). Taxonomic effects can vary between phyla and species and as such, it is often difficult to both identify any effect and to isolate the underlying physiological control (Weiner and Dove, 2003). As such, a species-specific palaeotemperature equation is likely to produce a more accurate reconstruction than a generic one.

The whelk, *Buccinum undatum*, is a marine gastropod species widely distributed throughout the North Atlantic (FAO, 2017). It is commercially important throughout much of its range (Heude-Berthelin *et al*., 2011), with the largest fishery located in UK waters with a total value of £21.9 million in 2018 (MMO, 2019). There are several potential methods for life history reconstructions in gastropods, including shells, statoliths, and opercula (Hollyman *et al*. 2018b). Determining age and growth is often crucially important in developing management strategies for commercially important species, to ensure their sustainable harvest (e.g. stock assessment; Vitale *et al*., 2019). Recent studies of this species have focussed on the development of age determination methods using the statoliths, to aid fisheries scientists in the monitoring of key populations (Hollyman *et al*., 2018a, Emmerson *et al*., 2019). Whilst rings in the internal statoliths provide a reliable method for determining individual age (Hollyman *et al*., 2018c), their use as environmental recorders appears to be limited as the incorporation of trace elements into the statoliths (such as Mg^{2+} and Sr^{2+}) is heavily influenced by vital effects (Hollyman *et al*., 2019). The isotopic composition of *B. undatum* shells was first studied by Santarelli and Gros (1985) who demonstrated seasonal cycles in $\delta^{18}O_s$ and compared these to the number of growth rings (annuli) on the organic opercula to validate the use of these structures in age determination. A similar approach was employed to validate the annual periodicity in statolith growth ring formation for this species, with their maximum longevity being ~10 years (Hollyman, 2017; Hollyman *et al*., 2018c). No previous work has reconstructed seawater temperatures in *B. undatum* shells using isotope data despite this species' wide distribution and commercial importance. As *B. undatum* is present in the fossil record as far back as the Pliocene (3.6 Ma; Behrensmeyer and Turner, 2017) and is occasionally found in Neolithic, Mesolithic and Palaeolithic shell midden assemblages throughout North Atlantic Europe (Thomas and Mannino, 1999; Dupont, 2006; Campbell and Russell, 2014), they

have the potential to be utilized in archaeological studies focussed on marine climate reconstruction.

The aim of the present study was to firstly confirm the structure and calcium carbonate polymorph of *B. undatum* shells as this is essential for interpreting isotope data. Secondly, a species specific palaeotemperature equation for this species was developed using laboratory-reared whelks to allow for accurate seawater temperature reconstructions. Lastly, shells of field-collected whelks were analysed and seawater temperatures reconstructed. These temperatures were then compared to instrumental data over the growth period to test their accuracy.

2 Materials and methods

2.1 Field sites and acquisition procedures for wild-caught shells

Three sample sites were chosen spanning the full latitudinal range of the U.K., the Shetland Isles (20 m depth, 60.64333° N, 0.9694444° W), the Menai Strait (11.5 m depth, 53.23389° N, 4.143056° W) and Jersey (13 m depth, 49.19333° N, 2.009167° W; Figure 1). Whelks were collected between the 9th and 27th of February 2015, using baited traps and sacrificed by freezing at –20 ^{o}C. When thawed, the bodies were removed from the shells which were cleaned in fresh water and left to dry at room temperature.

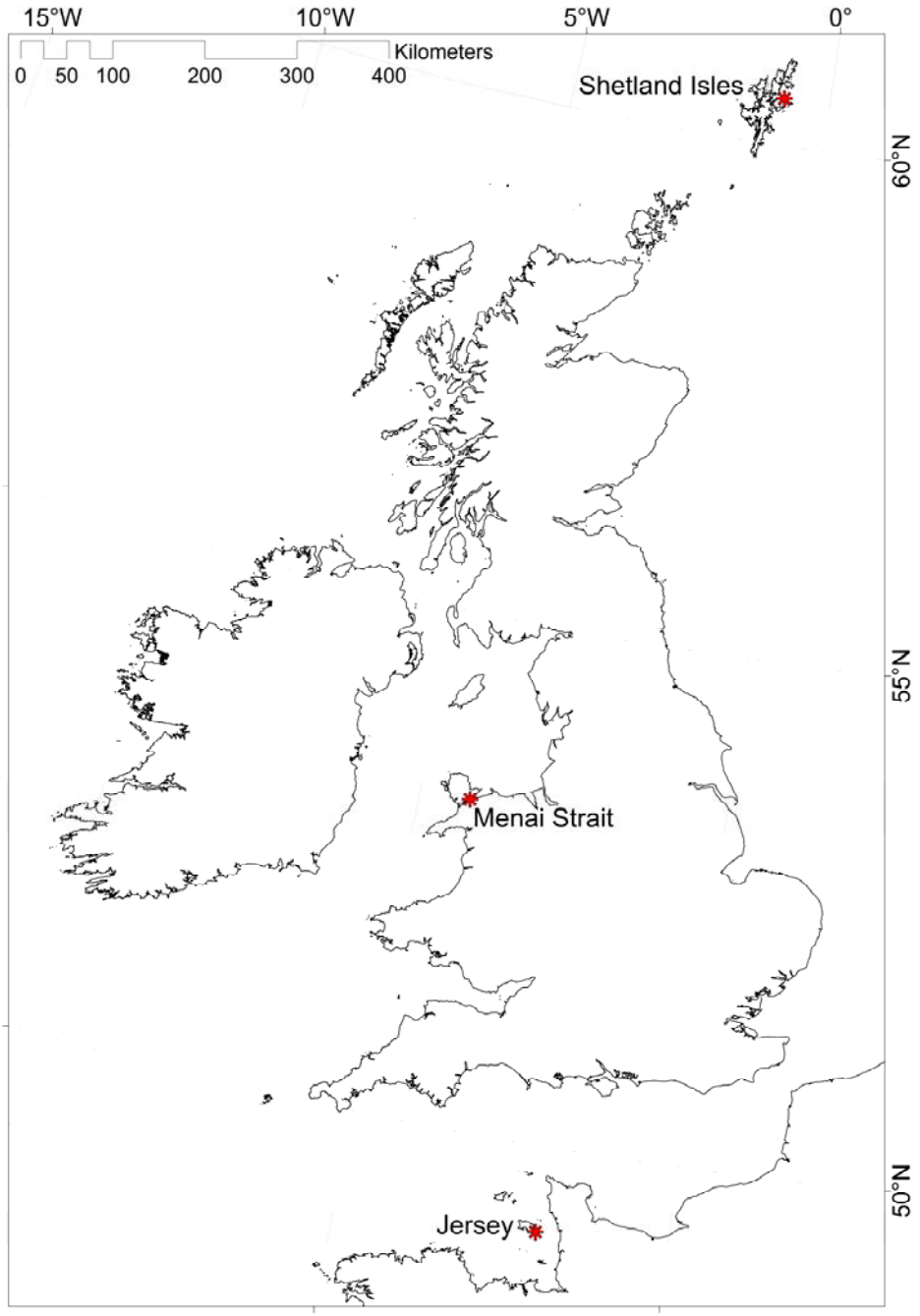

Figure 1. A map of the UK, highlighting the three sample locations for *B. undatum*.

2.2 Aquarium and experimental growth procedures

Juvenile *B. undatum* were hatched from egg masses collected on the 15th of November 2013 from Tal-y-Foel, North Wales, U.K. (53.158512° N, 4.279493° W). Egg cases and subsequent juvenile whelks were held in a laboratory aquarium for a period of 2 years in multiple 15 L tanks within a continuous flow system; this system was supplied with ambient seawater from the Menai Strait. Whelks were under an approximate 10:14 h light:dark cycle and fed pieces of mackerel

(*Scomber scombrus*) weekly or as required. Seawater temperatures within the aquarium were monitored throughout the 2-year growth period at three hourly intervals using a Tinytag™ Aquatic 2 temperature logger. Bi-monthly, three replicate seawater samples were removed from the centre of the aquarium in 25 ml LDPE bottles.

2.3 Shell microstructure analysis

Representative shells from the three sample sites were selected (3 from the Shetland Isles and Jersey and 6 from the Menai Strait, n = 12) and 1 x 2 cm shell sections from the shell lip and halfway up the growth axis were removed from each shell using a Dremel multitool with a cut-off attachment. The removed shell sections were embedded in Kleerset resin (Metprep) and left to cure for 72 hours. An Isomet 4000 precision saw (Buehler) was then used to section the resulting resin blocks to expose the internal layers of the shell. The resulting cut surfaces of the resin-shell blocks were ground and polished using silicon carbide grinding papers (FEPA P400, P1200 & P2500 grade) on a rotational grinder and a 3 µm diamond suspension. The polished surfaces were attached to microscope slides using superglue and superfluous resin and shell were sliced off the resin blocks to produce a ~1 mm thick section. These sections were ground and polished again to a thickness of ~100 µm. They were then imaged using a Meiji Techno MT8100 microscope with a Lumenera Infinity 3 microscope camera at 10× magnification.

Micro Raman Spectroscopy (MRS) was used to identify the calcium carbonate polymorph present in each structural layer of a representative shell from each sample site. For this technique, a resin-embedded shell from each site was sectioned across a region of interest (mid-height on the shell). The exposed cut shell surfaces were then polished as described above. The instrumental conditions for MRS were as follows: a 473 nm laser at a power of 15 mW was focussed using a lens with a magnification of 20× to provide excitation; Raman emission was observed using a grating with 2400 lines mm^{-1} and a pinhole size of 100 µm. Spectra between 135 and 750 cm^{-1} are presented as these are the wavelengths used to distinguish between calcium carbonate polymorphs (Wehrmeister *et al*., 2010a & b). Three sample spots were taken on each shell structural layer, these were then averaged to produce a single Raman spectra. Only the results from the Menai Strait shell are presented as equivalent results were found for the other 2 sites. Synthetic calcite and speleothem aragonite standards (Brinza *et al*. 2014) were analysed prior to shell analysis to define key interpretative bands. All Raman spectra were adjusted using a polynomial background correction.

2.4 Shell sampling procedures for isotope analysis

Shells of three adult male whelks (>70 mm total length) were selected for analysis from each of the three sample sites for an inter−site comparison (Figure 1) together with three adult females from the Menai Strait. The largest shells with low shell damage and fouling were selected to maximise the number of annual cycles for analysis and avoid confounding data from damaged shell sections. In February 2016 three of the largest 2-year old laboratory reared whelks (47, 42 & 51 mm measured from the apex to the tip of siphonal canal) were removed from the aquarium for isotopic analysis.

Shells were scrubbed clean to remove loose fragments of the organic periostracum as well as any attached debris or epiphytes and left to air dry. To maintain sampling consistency, a track of 2 mm increments was drawn on to the shell, roughly 5 mm from the shoulder of the shell whorl (Figure 2a). Although this distance varied depending on the size of each shell the same area and resolution were sampled each time. A 1 mm diamond burr drill was used to obtain discrete powder samples, considerable care was taken to only sample the outer shell layer. Powder samples were collected from ~1 cm long trenches every 2 mm around the entire whorl of the shell from the lip backwards. Sampling started at the second millimetre to avoid interference from the shell lip structure (Figure 2a). Sample trenches were made in line with visible striations on the surface of the shell structure (Figure 2b). Powder was collected on weighing paper and transferred to Eppendorf™ tubes for storage prior to analysis. As a pilot study, one shell (female, Menai Strait) was sampled at a consistent 2mm resolution and analysed using the methods described in section 2.5. Within the resulting pilot data 78 samples had been taken from within a single annual cycle (suggesting ~150mm linear shell growth in a single year), during the period of fastest growth (between the 2nd and 3rd shell whorls, Figure 2a). This was deemed to be excessive for the purposes of this study and for subsequent field collected shells, the sampling resolution was reduced to 4 mm over the same area. The shells used in this study were selected for minimal damage. However, where shell damage was obvious, the sample track was continued into the repaired area, and additional drilled samples were taken from the undamaged shell at the side of the repaired section. Using this sampling strategy the maximum amount of growth history was captured (Figure 2c). For laboratory reared whelks, a 2 mm sampling strategy was employed around the whole shell (apex to lip margin).

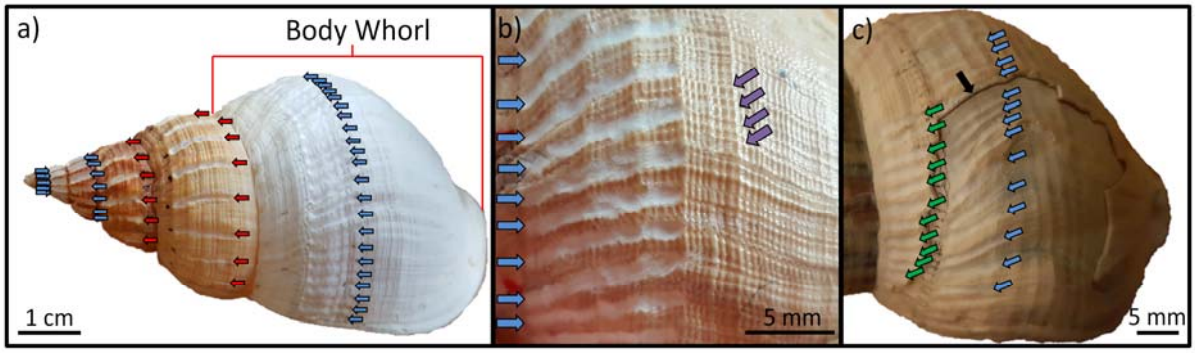

Figure 2. a) *Buccinum undatum* shell following drill sampling. Blue arrows represent a 2 mm sampling resolution whilst the red arrows represent a 4 mm sampling resolution. b) magnified image of the 2 mm resolution sample tracks (blue arrows) along visible shell striations (purple arrows). c) Sampling strategy across a shell damage incident (black arrow). Samples were taken along the original sampling path (blue arrows). However, samples were also taken along the pre-damage shell visible at the side of each damage area (green arrows) in order to fully reconstruct the growth history.

2.5 Isotope ratio mass spectrometry (IRMS)

An Isoprime dual inlet mass spectrometer and Multiprep device were used at the British Geological Survey, for all shell isotope analyses. 50−100 µg of the powdered sample was weighed, added to a glass vial and sealed with a rubber septa and lid. The sample vials were evacuated and anhydrous phosphoric acid (H_3PO_4) added to each sample at 90°C. Samples were left to digest for 15 minutes and the expressed gas (mainly comprised of CO_2) was collected and cryogenically cleaned to remove any moisture before mass spectrometry. Instrumental drift in measured ratios was accounted for by analysing a laboratory standard (Keyworth Carrara Marble (KCM), VPDB $\delta^{18}O$ = −1.73 ‰) before, during and after each run. KCM has been calibrated against NBS-19, (Friedman *et al*., 1982; VPDB $\delta^{18}0$ = -2.20‰). Isotope values ($\delta^{18}O_s$) are reported against the VPDB (Vienna Pee Dee Belemnite) standard. The Craig correction (Craig, 1957, Electronic appendix, equation 1 & 2) was then applied to the data and the resulting isotopic ratios of the samples are expressed in delta units, $\delta^{13}C$ and $\delta^{18}O$ (‰, parts per mille). The calculated total error on all standards was as follows: $\delta^{13}C$ VPDB = ±0.03‰, $\delta^{18}O$ VPDB = ±0.05‰ (n = 238, 1σ). The fractionation factor for aragonite digested at 90°C was then applied to the data (Sharma and Clayton, 1965; Kim *et al*., 2007).

Seawater samples were processed using the CO_2 equilibration method with an Isoprime 100 mass spectrometer plus Aquaprep device (also at the British Geological Survey) to determine bi-monthly the $\delta^{18}O$ of the seawater ($\delta^{18}O_w$) during growth and development of the whelks. 200 µl of each seawater sample was pipetted into a Labco Exetainer® vial and heated to 40°C in a sample tray. Any gas present in the vials was removed, flushed with CO_2 and left to equilibrate for 12 hours. A cryogenic water trap was then used to remove any moisture from each equilibrated gas

sample. The dry sample gas was analysed using the IRMS. Two laboratory standards (CA−HI (δ^{18}0 SMOW=-7.30‰) and CA−LO (δ^{18}0 SMOW=-39.30‰)) plus two secondary standards were analysed in each run. Each laboratory standard was calibrated against reference materials (VSMOW2, SLAP2 and GISP) so the resulting $^{18}O/^{16}O$ ratios of the samples ($\delta^{18}O_w$) were calculated and expressed in delta units, $\delta^{18}O$ against the VSMOW scale. Errors are typically +/− 0.05 per mil.

2.6 Data analysis

2.6.1 Palaeotemperature equation calculation

A species-specific palaeotemperature equation was calibrated using aquarium $\delta^{18}O_w$ and $\delta^{18}O_s$ values from the laboratory reared whelks, with seawater temperature data from the Tinytag logger. The calculation compares seawater temperature to $\delta^{18}O_s$ - $\delta^{18}O_w$ and uses regression analysis to calculate a linear relationship. Ranged Major Axis (RMA) regression analysis was used to account for potential error on both the x and y axes with the lmodel2 package (Legendre, 2017) in R (version 3.6.2; R core team 2019).

2.6.2 Average isotope profiles of field collected whelks

Available seawater temperature data were obtained for each sample collection location between October 2011 and January 2015 (CEFAS−the Menai Strait, Marine Scotland−Shetland, Jersey Department of the Environment−Jersey). Following this, each individual whelk $\delta^{18}O_S$ profile was aligned to the seasonal cycle of the site-specific seawater temperature by anchoring the dates of the maxima and minima of the seawater temperature profile to the minima and maxima in the $\delta^{18}O_s$ profile (as $\delta^{18}O_s$ is inverse to seawater temperature). Dates were then interpolated between the anchored dates. Next, average $\delta^{18}O_S$ profiles were created for each site by compiling all the isotope profiles from a single site into one average profile in MATLAB (ver. 9.0). Data were interpolated onto the first day of each calendar week (or each day depending on the resolution required) using a cubic spline, all the $\delta^{18}O_S$ values for the same interpolated date were averaged to a single value.

2.6.3 Sensitivity analysis

Subsequently, the resulting average $\delta^{18}O_S$ profiles were converted to seawater temperature values using the newly calibrated palaeotemperature equation and plotted against the measured sea surface temperature (SST) from each site. *In-situ* $\delta^{18}O_w$ values for each site were unavailable for the whole time period, to compensate for this a sensitivity analysis was

undertaken to determine the most likely values of $\delta^{18}O_w$ to use in reconstructions at each site. $\delta^{18}O_w$ values ranging from –1 to 1 ‰ with 0.25 steps were chosen based on $\delta^{18}O_w$ values from this study as well as those in the literature (Hermoso *et al*., 2016; McKenna *et al*., 2016). For each 0.25 step in $\delta^{18}O_w$, palaeotemperature was reconstructed for the average $\delta^{18}O_S$ profiles. The average deviation of the reconstructed temperature from recorded seawater temperature over the whole period of growth was calculated using the following equation:

$$\sum \frac{\text{reconstructed seawater temperature } (^{o}C)}{\text{observed seawater temperature } (^{o}C)} / \text{n} \quad [1]$$

The resulting values were then compared to find the lowest deviation from observed seawater temperature.

2.6.4 Investigations of vital effects

To test for the presence of a kinetic effect, the correlation between $\delta^{13}C_S$ and $\delta^{18}O_S$ was tested for each individual shell, along with a linear regression analysis to estimate R^2 values. $\delta^{13}C_S$ and $\delta^{18}O_S$ may both deplete when a kinetic effect is present, leading to a quasi-linear relationship between the two sets of values (McConnaughey, 1989a & b; Flores et al., 2018). All analyses were performed in R (version 3.6.2).

With the aim of identifying any offset caused by a species specific or taxonomic vital effect, expected values for $\delta^{18}O_s$ were calculated by re-arranging the palaeotemperature equation derived from Kim *et al*., (2007; described in section 2.6.5) and using observed seawater temperature and estimated $\delta^{18}O_w$ (outlined earlier). Resulting estimated $\delta^{18}O$ values ($\delta^{18}O_{est}$) were then compared with corresponding $\delta^{18}O_s$ values to calculate any offset. The Kim *et al*., (2007) equation was chosen as it was calculated using a biogenic aragonite and so the resulting $\delta^{18}O_{est}$ values would represent isotopic equilibrium at a chosen temperature whilst discounting vital effects.

2.6.5 Comparison to existing palaeotemperature equations

To compare differences between the newly calculated equation and previously published equations, raw data (temperature, $\delta^{18}O_w$ and $\delta^{18}O_s$) were extracted from several key papers which calibrated their own equations. Studies were chosen based on the type of material analysed to allow comparisons to be made to the data presented here. Following the necessary conversions

between isotopic scales outlined below, differences between palaeotemperature equation data were investigated using ANCOVA in R (version 3.6.2; R core team 2019). Differences in both slope and intercept were analysed using pairwise comparisons. Residuals were checked for a random distribution around zero, quantile plots were also checked for an approximately symmetrical normal distribution.

Four established equations were used for comparison in this study, Epstein *et al*., (1953) was chosen as an early example which utilized a mix of biogenic calcite and aragonite. Grossman and Ku, (1986) was chosen as example of biogenic aragonite (both the molluscan only and combined molluscan and foraminifera data from this study are used). Kim and O'Neil, (1997) was chosen for their analysis of abiogenic calcite. Kim *et al*., (2007) was chosen as they analysed abiogenic (synthetic) aragonite. As the $\delta^{18}O_w$ data from both Epstein *et al*., (1953) and Grossman and Ku, (1986) were presented against the PDB scale, they had to be converted to VSMOW using the following equation (Equation 2, Friedman and O'Neil, 1977):

$$\delta^{18}O_w \text{ (VSMOW)} = 1.00022 \times \delta^{18}O_w \text{ (PDB)} + 0.22 \quad [2]$$

Similarly, the $\delta^{18}O_s$ data from Kim and O'Neil, (1997) and Kim *et al*., (2007) were presented against the VSMOW scale and so were converted using the following equation (Equation 3, Kim *et al*., 2015):

$$\delta^{18}O_s \text{ (VPDB)} = 0.97001 \times \delta^{18}O_s \text{ (SMOW)} - 29.99 \quad [3]$$

The $\delta^{18}O_s$ data from Kim and O'Neil, (1997) were also adjusted to account for a different calcite acid fractionation factor used (1.01050) for better comparison to the other datasets (after Wanamaker *et al*., 2006). This equation was also reorganised by Leng and Marshall (2004), however the difference in acid fractionation factor was not accounted for (as it was not necessary within the context of their study), therefore the Wanamaker *et al*. (2006) expression of the data was used here. Similarly, the $\delta^{18}O_s$ data from Kim *et al*., (2007) were adjusted to account for a different aragonite acid fractionation factor used (1.01063) for better comparison to the data from this study.

3. Results

3.1 Shell structure and composition

Four aragonitic shell layers were identified in the cross section of *Buccinum undatum* shells (Figure 3) with obvious differences in microstructure and crystal orientation: an outer prismatic layer, two internal crossed-lamellar layers (1 & 2) and an internal hypostracum (H). The hypostracum is not present in newly formed shell at the growing edge suggesting it forms after the outer three layers, potentially as a strengthening mechanism over time. An outer organic periostracum was observed on all shells although it was thin, and was scrubbed off prior embedding to ensure resin adherence. All shell layers were devoid of any identifiable annual lines either externally or internally in cross sections.

To avoid cross contamination with the inner and visibly different layers all isotope drill sampling was undertaken in the outer prismatic layer (P). No regular (potentially annual) visible growth lines were found in any of the shells. Whilst there are clear visible differences in the crystal structures between layers, from the Raman spectra all the layers are composed of aragonite when compared to aragonite and calcite standards (Figure 4). Clear peaks were seen at characteristic wavelengths for aragonitic structures (151, 206 and 702-706 cm^{-1}, Parker *et al*., 2010). A clear matching characteristic calcium carbonate peak was also found at 1085 cm^{-1} (Parker *et al*., 2010). The same results were found for all analysed shells from all sites. This unanimity of data allowed a consistent fractionation factor to be applied for all sample data following IRMS.

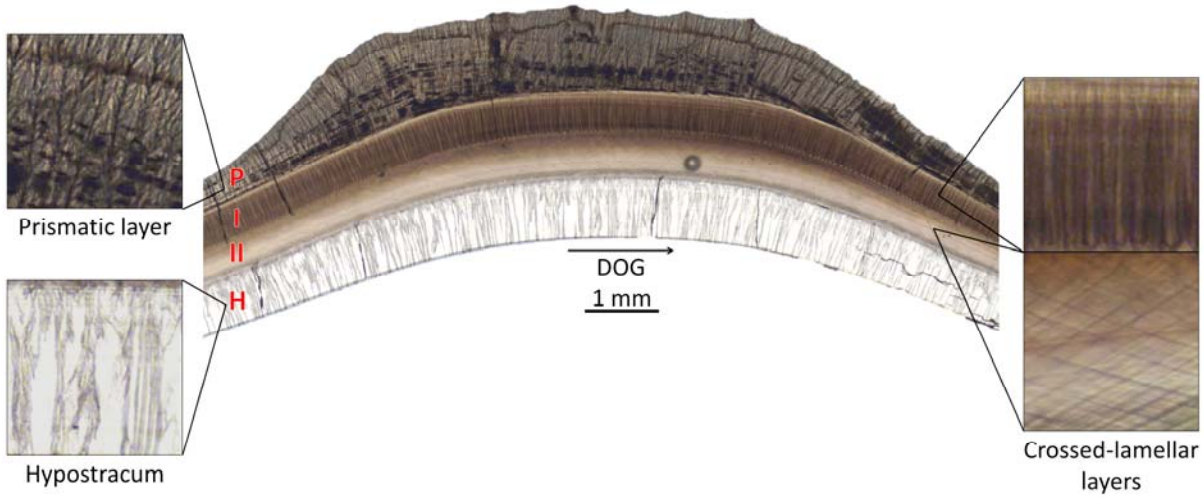

Figure 3. Photomicrograph montage of a thin shell section from an adult *Buccinum undatum* shell collected from the Menai Strait. The section has been prepared parallel to the growth axis. There are distinctive differences in crystal structure visible between the four different layers observable in the inset images. DOG = Direction of Growth. P = prismatic Layer, I = crossed-lamellar layer 1, II = crossed-lamellar layer 2, H = hypostracum.

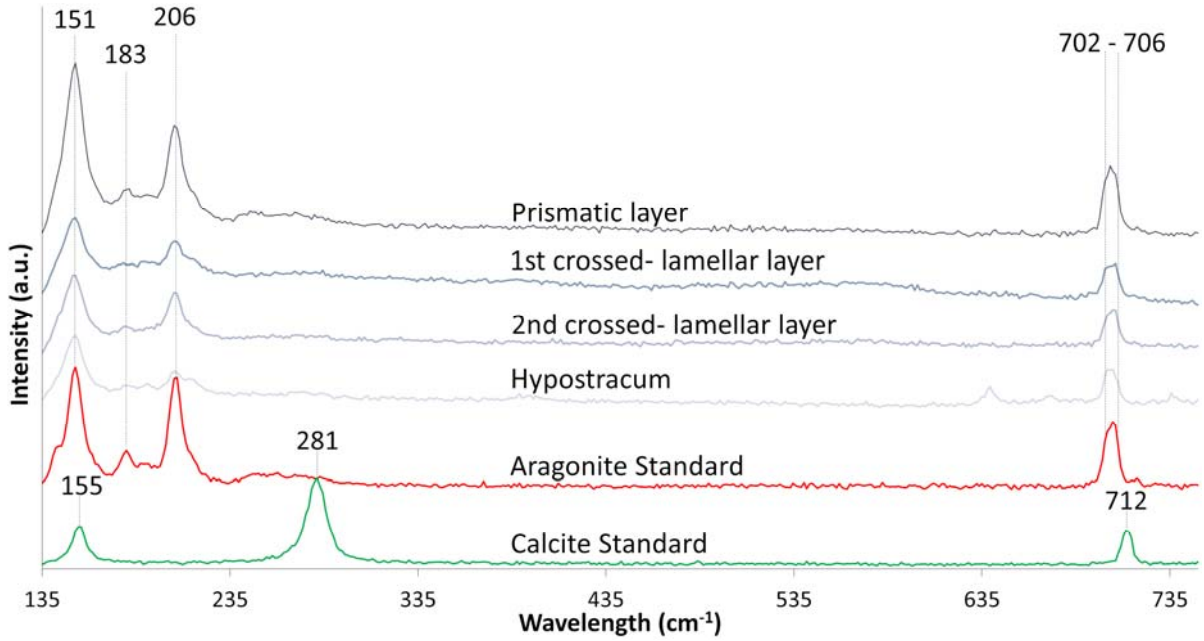

Figure 4. Raman spectra between 135 and 750 cm^{-1} for four shell layers, the prismatic layer, 1st and 2nd crossed-lamellar layers and nacreous layers from a shell section of *Buccinum undatum* from the Menai Strait. Characteristic peaks in the spectra are indicated (dotted lines) for both calcite and aragonite. There is clear agreement between the four shell layers and the aragonite standard. Y axis = arbitrary units.

3.2 Species Specific Paleotemperature Equation

The $\delta^{18}O_s$ profiles from each of the three laboratory reared 2 year old *B. undatum* shells were assigned dates and matched to $\delta^{18}O_w$ values with the same dates. $\delta^{18}O_s - \delta^{18}O_w$ was then compared with aquarium seawater temperature over the same time period. Regression analysis was used to derive the following species specific palaeotemperature equation (Equation 5, r^2 = 0.94).

$$t(^{o}C) = 14.96 (\pm 0.15) - 4.94 (\pm 0.22) \times (\delta^{18}O_{shell} - \delta^{18}O_{water}) \quad [4]$$

3.3 Site SST profiles

Seasonal sea surface temperature (SST) profiles from the Menai Strait, Jersey and Shetland covering a 4.5 year period are shown in Figure 5. The northerly Shetland Isles was the coldest of the three sites. The Menai Strait and Jersey have similar seasonal seawater temperature cycles, although the Menai Strait reached lower seawater temperatures in the winter (4 °C) (comparable to those around Shetland) than Jersey (7 °C). Jersey coastal waters reached slightly higher

maximum temperatures (18.5 °C) and stayed warmer for longer between the summer maximum and the winter minimum.

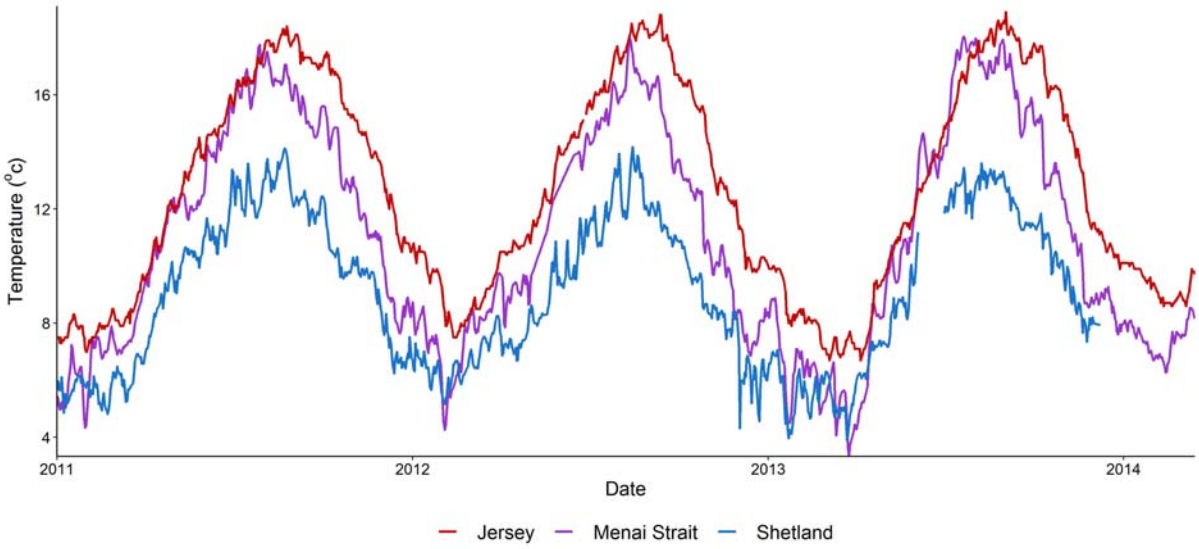

Figure 5. Daily recorded sea surface temperature (SST) records between February 2011 and February 2014 from the three main study sites. Gaps in the Shetland and Menai Strait data were due to temperature logger failures. Data were obtained from Marine Scotland (Shetland), Department of the Environment (Jersey) and CEFAS (Menai Strait).

3.4 Sensitivity analysis

Table 1 presents the results of the sensitivity analysis. An average $\delta^{18}O_w$ value for Menai Strait water of 0.01 ‰ was also used in the sensitivity analysis (average value of all of the $\delta^{18}O_w$ samples analysed in this study). The values with the smallest deviation were used in the palaeotemperature reconstruction on a site-by-site basis (Jersey 0.75; Menai Strait 0.01; Shetland 0.25).

Table 1. Results of a sensitivity analysis to determine the most likely $\delta^{18}O_w$ values to use in the seawater temperature reconstructions from Jersey, the Menai Strait and Shetland. The values with the lowest deviation are highlighted in bold. The 0.01 value (in italics) was calculated from $\delta^{18}O_w$ values from Menai Strait derived seawater samples.

	$\delta^{18}O_{water}$ (‰)											
	–1	–0.75	–0.5	–0.25	0	***0.01***	0.25	0.5	0.75	1	SD	SE
Shetland	5.81	4.58	3.34	2.11	0.82	0.87	**-0.09**	-1.60	-2.84	0.38	2.51	0.06
Menai Strait	5.10	3.87	2.63	1.40	0.16	**0.11**	-1.08	-2.31	-3.55	-4.78	1.93	0.05
Jersey	8.52	7.29	6.05	4.82	3.52	3.58	2.34	1.11	**-0.13**	-1.36	1.46	0.04

3.5 Seawater temperature reconstructions from field collected *Buccinum undatum*

The age of the sampled whelks (calculated from the number of clear $\delta^{18}O_S$ cycles) ranged between 3 (Menai Strait) and 7 (Shetland) years old. The seawater temperature reconstructions for the three sites are shown in Figure 6. The black bars below each plot represent the number of shells included in the average profile at any one point, portions of the average profile which only represent a single shell are not presented. It is clear from the plots that the reconstructions from Jersey and the Menai Strait have roughly the same temperature range as their observed SST counterparts (88.3 % and 78.8 % of the same range respectively). However, the reconstruction for Shetland has a temperature range that only covers 62.5 % of the SST range (Figure 6).

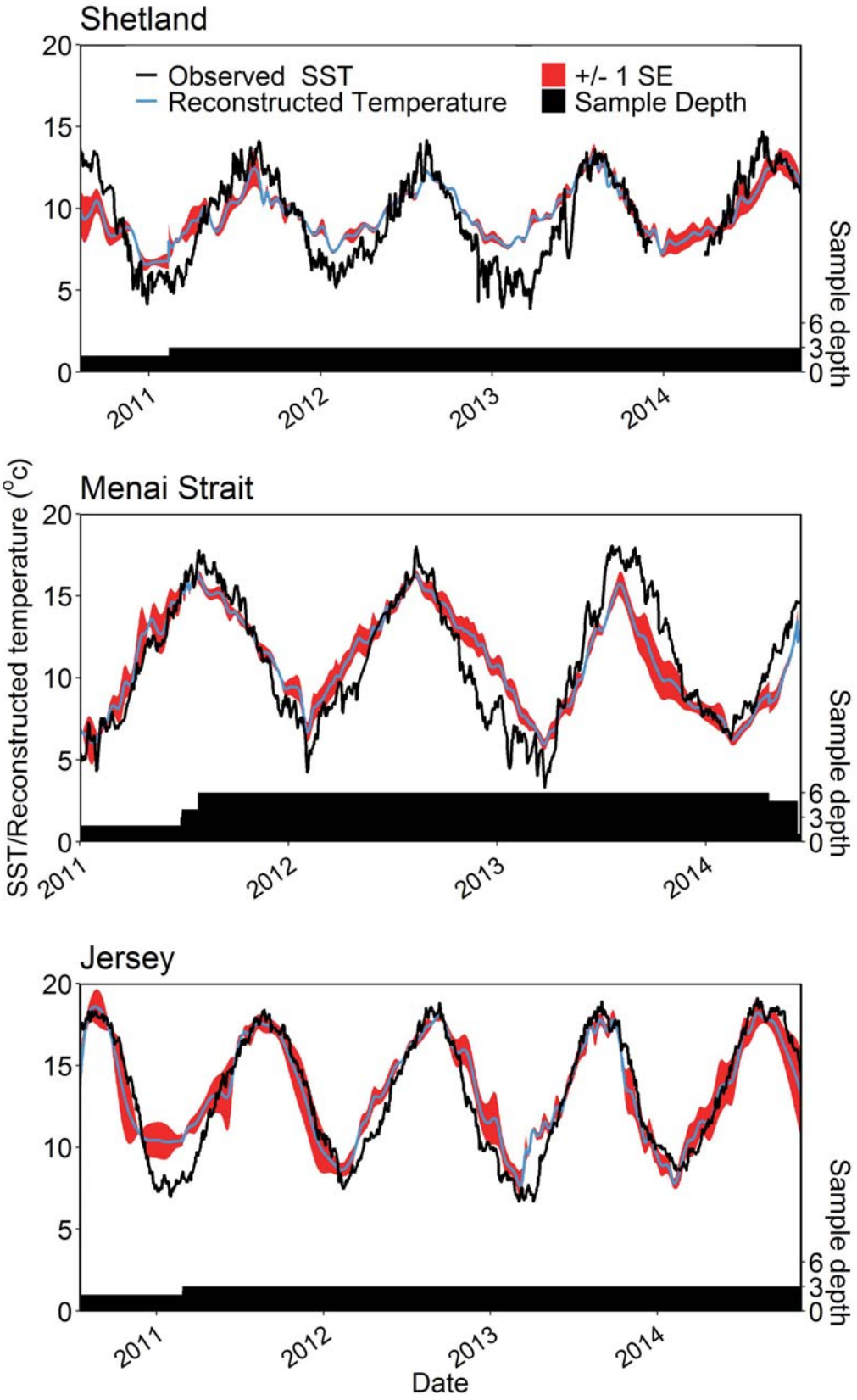

Figure 6. Daily observed seawater temperature from the Shetland Isles (top), Menai Strait (middle) and Jersey (bottom) overlaid with the reconstructed temperature from the average isotope profile from each respective area (grey line). Shaded grey areas indicate +/– 1SE. The sample depth (number of shells contributing to the average value at any point) is shown at the bottom of each plot.

399 3.6 Vital effects

400 No kinetic effects were evident in the comparison of $\delta^{13}C_S$ and $\delta^{18}O_S$. Whilst some shells did
401 display a significant correlation indicating the possibility of kinetic disequilibrium, none were
402 more than moderate in strength (maximum 0.48; Electronic Appendix: Table A, Figure A). Of the
403 relationships that were significant, some displayed a positive relationship and some a negative.

404 A positive offset between expected (calculated using Kim et al., 2007) and observed $\delta^{18}O_s$
405 values was found ($\delta^{18}O_{est}$ - $\delta^{18}O_s$). There was a similar average offset at each site (1.01 – 1.06‰)
406 with an overall offset of 1.04 ‰ (± 0.41 ‰). Whilst the average offset at each site was similar,
407 there was a high degree of variability within these estimates. Importantly, this suggests that the
408 offset is not constant throughout the year. To investigate this further, the offsets ($\delta^{18}O_{est}$ and
409 $\delta^{18}O_S$) were compared to observed SST values. All comparisons resulted in significant positive
410 correlations (Table 2, Electronic Appendix, Figure B), with larger differences between observed
411 and expected $\delta^{18}O$ values occurring at the lower extremes of the temperature range, this is also
412 seen in Figure 6.

413 Table 2. Offset values ($\delta^{18}O_{est}$ - $\delta^{18}O_s$) for each individual shell along with combined values for each site. The
414 relationship between seawater temperature and the offset for each individual shell can be seen on the right of
415 the table, raw data from these comparisons can be seen in Electronic Appendix, Figure B. Bold values indicate a
416 significant result.

				Temperature vs. Offset			
Location	Sample	Offset	*n*	corval	r^2	Intercept	Slope
Shetland	1	0.96 (±0.37)	93	**-0.88**	0.77	**15.77**	**-6.61**
	2	1.1 (±0.35)	96	**-0.74**	0.55	**15.67**	**-5.48**
	3	1.07 (±0.38)	100	**-0.73**	0.53	**15.25**	**-5.30**
	Combined	1.04 (±0.37)	289				
Menai Strait	1	1.29 (±0.47)	145	**-0.68**	0.46	**18.31**	**-5.52**
	2	1.13 (±0.51)	98	**-0.57**	0.33	**15.50**	**-4.29**
	3	1.01 (±0.39)	93	**-0.72**	0.53	**18.62**	**-7.48**
	4	0.98 (±0.45)	93	**-0.52**	0.27	**15.98**	**-4.55**
	5	0.76 (±0.31)	99	**-0.71**	0.50	**17.92**	**-8.61**
	6	1.06 (±0.4)	106	**-0.60**	0.36	**16.96**	**-5.66**
	Combined	1.06 (±0.46)	634				
Jersey	1	0.88 (±0.39)	92	**-0.50**	0.25	**17.30**	**-4.72**
	2	1.15 (±0.26)	90	**-0.60**	0.36	**22.87**	**-8.46**
	3	1.02 (±0.37)	99	**-0.60**	0.36	**18.92**	**-5.89**
	Combined	1.01 (±0.36)	281				
Tank	1	0.98 (±0.21)	64	**-0.58**	0.34	**21.85**	**-9.59**
	2	1.08 (±0.32)	63	**-0.45**	0.20	**17.60**	**-4.85**
	3	1.06 (±0.29)	58	**-0.26**	0.07	**15.51**	**-3.04**

	Combined	1.04 (±0.28)	185

With the knowledge of the offset, it is possible to amend the $\delta^{18}O_S$ data to compensate for this. The species specific equation still produces a more accurate reconstruction using the original $\delta^{18}O_S$ data than the Kim using offset corrected $\delta^{18}O_S$ values (Table 3).

Table 3. Average deviation of reconstructed from observed seawater temperatures for the equations derived from this study and Kim *et al.*, (2007) using the calculated vital offset.

Site		This Study	Kim *et al.*, (2007) with offset
Shetland	Average deviation (^{O}C)	–0.37	–2.37
	StDev	2.51	2.51
	StErr	0.06	0.06
Jersey	Average deviation (^{O}C)	–0.13	0.37
	StDev	1.46	1.46
	StErr	0.04	0.04
Menai	Average deviation (^{O}C)	0.20	0.55
	StDev	1.92	1.92
	StErr	0.05	0.05

4 Discussion

4.1 Palaeotemperature equation calibration

The newly calibrated *B. undatum* equation [4] differs from key palaeotemperature equations derived from the published literature (Figure 7). Comparisons between published palaeotemperature calibrations and the *B. undatum* data show that the calibrated equation of this study has a significantly different intercept to all other equations (Electronic Appendix Table B). The only significantly different slopes (at the 95 % confidence interval) to the *B. undatum* calibration were that of Grossman and Ku (1986, combined molluscan aragonite and foraminiferal material) and Epstein *et al.*, (1953, mix of biogenic aragonite and calcite).

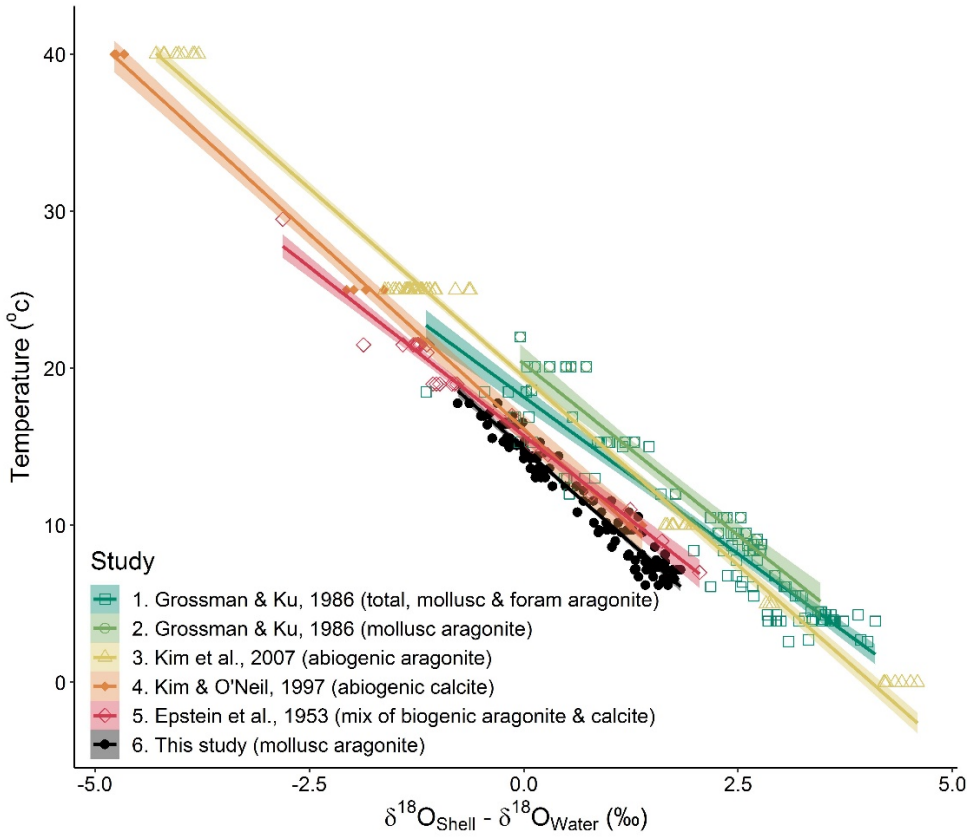

433

434 Figure 7. Linear relationship between seawater temperature and $\delta^{18}O_{shell} - \delta^{18}O_{water}$ for the data obtained from
435 *Buccinum undatum* shells (black dots/line) as well as the literature. Shaded areas represent 95 % confidence
436 intervals.

437 A three-year period of $\delta^{18}O_S$ from the wild caught Menai Strait samples was used to assess
438 the accuracy of the new equation. This time period and sample site were chosen as the juvenile
439 whelks used for the calibration were grown in an aquarium fed with water from the Menai Strait.
440 With only 0.11°C average deviation from observed seawater temperature, the new calibration
441 displays the best fit (Electronic appendix, Table C). The temperature range of the reconstructed
442 profiles was also the best using the newly calibrated equation (78.79 %). A commonly used
443 palaeotemperature equation for aragonite shell (both bivalves and gastropods) is the Grossman
444 and Ku (1986) calibration, which was originally calculated using biogenic aragonite and has been
445 used in a number of studies e.g. Sosdian *et al*., (2006); Schöne *et al*., (2007); Reynolds *et al*.,
446 (2013). When this equation was used to calculate the seawater temperatures for the aragonitic
447 *B. undatum* shells in this study, seawater temperature was significantly overestimated (Electronic
448 appendix, Table C). The most similar reconstruction was produced by the Epstein *et al*., (1953)
449 equation, which is based on a mix of biogenic calcite and aragonite. However, we have definitively
450 confirmed using Raman spectroscopy that *B. undatum* shells are wholly aragonite.

451 4.2 Reconstruction of palaeotemperature from field collected shells

452 The species specific *B. undatum* temperature equation produced the closest match to the
453 observed seawater temperatures for the selected three-year period of data from the Menai Strait;
454 an 0.2°C average deviation and a profile which covered 78.8 % of the observed seawater
455 temperature range. This new equation was then applied to the average $\delta^{18}O_S$ profiles from Jersey
456 and Shetland and the reconstructions covered 88.3 % and 62.5 % of the observed seawater
457 temperature ranges respectively.

458 The Shetland reconstruction was the least accurate and there are several possible
459 explanations for this. Firstly, the $\delta^{18}O_w$ calculated during the sensitivity analysis was inaccurate.
460 This is unlikely as the calculated value for Shetland (0.25) fell within the range of isotope values
461 in seawater samples from the Faroe–Shetland channel during the period between 2009 and 2013
462 (0.04–0.6, McKenna *et al*., 2016; B. Berx, Marine Scotland, Pers. Comm.). The channel is roughly
463 160 km away from the study site but may well have an influence there due to strong current flows.
464 It is therefore likely that the $\delta^{18}O_w$ values at this site vary annually by analogy with other sites. It
465 is common practice to use a single $\delta^{18}O_w$ value during a palaeotemperature reconstruction when
466 higher resolution $\delta^{18}O_w$ data are unavailable (e.g. Hermoso *et al*., 2016). The measured $\delta^{18}O_w$
467 values from the Menai Strait used in the palaeotemperature calibration of whelk shells from this
468 location did not exhibit a clear annual cyclicity. This is similar to the findings of Owen *et al*.,
469 (2002b) who found no annual cycle in the $\delta^{18}O_w$ profile of Menai Strait seawater.

470 A second possible explanation for the poor accuracy of the Shetland reconstruction is that
471 the temperature range experienced by the whelks from Shetland was less than that recorded in
472 surface waters by the SST logger. Significantly, the whelks from Shetland were obtained from a
473 site deeper than either the Menai Strait or Jersey and so may have been buffered from the
474 temperature extremes recorded in the surface waters by the logger, resulting in an isotopic profile
475 with a lower amplitude than the observed SST profile.

476 The final possible explanation for the poorer seawater temperature reconstruction
477 observed in the Shetland whelks may be because there was a cessation of growth during the
478 winter seawater temperature minima. It is likely that the growth of *B. undatum* slows or even
479 ceases during the cold winter season as their metabolism drops below a critical level. This has
480 been observed in many mollusc species (Lutz and Rhoades, 1977; Schöne *et al*., 2005) and often
481 results in the formation of a growth line or annulus in the shell (Richardson, 2001). We have

observed that the growth rates of laboratory reared *B. undatum* slow in seasonally colder seawater temperatures (Hollyman *et al*., 2018c), although it is not yet known whether there is complete cessation of growth during these cold periods or just a decrease in growth rate. In the Menai Strait, the observed seawater temperatures were as cold as those in the Shetlands, yet the seawater temperature reconstructions in the Menai Strait whelks more closely matched the measured seawater temperature, so it is less likely an explanation as this phenomenon was not apparent at this site. To investigate this disagreement further, in future studies $\delta^{18}O_w$ and seawater temperature data from the Shetland site could be obtained regularly over an annual cycle and compared to $\delta^{18}O_S$ values from whelks collected over the same time period.

Whilst better than the reconstruction in Shetland, the imperfect reconstructions seen in the Menai Strait and Jersey also raise the same questions about the source of inaccuracy. In both these cases, seawater temperature data were obtained from a comparable location; and for the Menai Strait, $\delta^{18}O_w$ was available for some of the growth period. In these cases the inaccuracy may be a result of population level differences in environmental tolerance. As whelks do not migrate over large distances and display low dispersal between populations they can form isolated stocks (Fahy *et al*., 2000; Weetman *et al*., 2006; Magnúsdóttir *et al*., 2019). Therefore, local adaptations may be present in their biological tolerances and subsequent growth rates under certain temperatures. The methods used to anchor dates to the $\delta^{18}O_S$ profiles and the subsequent interpolation and averaging may have had a smoothing effect on the resulting data. With no visible annual lines to use as markers in the shell, this was the only obvious way to achieve the desired average temperature profiles. Future studies could investigate similar methods of achieving the same effect whilst preserving more of the variability in the data.

4.4 Disequilibrium of observed $\delta^{18}O_{Shell}$

No obvious or reliable kinetic disequilibrium was observed in the data, with both weak – medium positive and negative correlations seen between $\delta^{13}C_S$ and $\delta^{18}O_S$. When kinetic disequilibrium is evident, heavier isotopes (^{18}O & ^{13}C) may deplete as they are preferentially incorporated during periods of fast growth, leading to a quasi-linear relationship between $\delta^{13}C_S$ and $\delta^{18}O_S$ (McConnaughey, 1989a & b). $\delta^{13}C_S$ is often thought to be representative of dissolved inorganic carbon in the water column and as such, may be a proxy for ocean productivity (Spero *et al*., 1997; Goodwin *et al*., 2013). There may also be vital effects influencing $\delta^{13}C_S$ with carbon from metabolic sources such as respiration and digestion often contributing to $\delta^{13}C_S$ in marine

513 molluscs (e.g. Owen *et al*., 2002a & b). As *B. undatum* is a scavenging predatory gastropod, able
514 to feed on a wide variety of prey species (Hancock, 1960; Scolding *et al.*, 2007), carbon sourced
515 from digestion may be highly variable between individuals, which may explain the high variability
516 in the relationship between $\delta^{13}C_S$ and $\delta^{18}O_S$ amongst specimens (Electronic appendix, Table A,
517 Figure A). Metabolically sourced carbon may also be potentially masking a kinetic disequilibrium
518 effect and therefore future controlled laboratory feeding experiments could address this
519 question.

520 An offset of 1.04 ‰ (± 0.4 ‰) between $\delta^{18}O_{exp}$ and $\delta^{18}O_S$ appears to be present in the data
521 due to a vital effect, although it is unclear specifically what this may be. This offset is the likely
522 cause of the difference between the species-specific equation and previous aragonite based
523 equations (Figure 7). The magnitude of this offset is similar to previous offsets reported for several
524 other gastropod species, specifically limpets which are often used in archaeological studies (e.g.
525 *Fissurella maxima* –1 ‰ [Flores *et al*., 2018]; *Patella caerulea* –0.72 ‰ [Prendergast and Schöne,
526 2017]; *Patella vulgata* –1.01 ‰ [Fenger *et al*., 2007]). However, the offset in *B. undatum* is a
527 positive difference between $\delta^{18}O_{exp}$ and $\delta^{18}O_S$ (i.e. observed $\delta^{18}O$ values are more negative than
528 expected) in contrast to the negative offsets reported for limpets. The limpet shell material used
529 in these studies was calcite, not aragonite, which may explain the large difference between the
530 absolute offset values.

531 Several studies have also identified positive offsets in bivalve shells with a calcite
532 composition, such as *Mytilus californianus* (0.2 – 0.5‰, Ford *et al*., 2010), *Comptopallium radula*
533 (~0.7‰, Thébault *et al*., 2007) and *Pecten maxiumus* (0.4 – 0.6‰, Owen *et al*., 2002a & b).
534 Multiple explanations have been suggested for the observed positive offsets in these species.
535 Firstly, the metabolic control of pH within the extra-pallial fluid (EPF – the medium from which
536 calcium carbonate is precipitated during shell formation [Wilbur and Saleuddin, 1983]). Differing
537 pH has been shown to result in fractionation between $\delta^{18}O_{carbonate}$ and $\delta^{18}O_{water}$ in both scallops
538 and foraminifera (Spero *et al*., 1997; Zeebe, 1999; Owen *et al*., 2002b; Thébault *et al*., 2007). It is
539 unknown whether the pH of the EPF within *B. undatum* differs from seawater, but if so, this could
540 be a viable explanation for the offset observed in this study. However, Kim *et al*. (2006) concluded
541 that isotopic fractionation in aragonite is independent of pH, making this theory unlikely. A second
542 proposed explanation is that of Rayleigh fractionation, which can occur in a closed system with a
543 finite reservoir (i.e. the EPF)(Thébault *et al*., 2007). This theory assumes the reaction removing
544 material from the reservoir (i.e. calcification) is causing fractionation, and any reaction is not

reversed (e.g. the carbonate does not dissolve/recrystallize after the initial formation)(Thébault *et al*., 2007). The continual removal of material from the reservoir then results in a shift in the $\delta^{18}O$ of the reservoir and carbonate. This effect has been demonstrated during the evaporation of water (Kendall and Caldwell, 1998) and has been proposed as a reason for $\delta^{18}O$ offsets in speleothems (Mickler *et al*., 2004). This explanation assumes the EFP of *B. undatum* is largely isolated from surrounding seawater, something which has not been confirmed. Lastly, the offset between $\delta^{18}O_{exp}$ and $\delta^{18}O_S$ could simply be due to differing $\delta^{18}O$ values of the EPF and seawater caused by a physiological control of the EPF composition (Thébault *et al*., 2007), which again assumes that the EPF is *B. undatum* is isolated from seawater. It is difficult to conclude which mechanism (if any outlined here) may be controlling the offset observed in *B. undatum*. This is due to a lack of knowledge around the specific process of calcification in this species and whether it is similar to the model proposed by Wilbur and Saleuddin (1983) for bivalves. Further detailed studies on the process of calcification in *B. undatum*, alongside concurrent measurement of EPF, $\delta^{18}O_S$ and $\delta^{18}O_w$ composition would clarify this.

The cause of the offset is unclear but appears to be a taxonomic (i.e. species specific) vital effect linked to growth rate. The positive offset observed in *Pecten maximus* was also shown to vary depending on growth rate (Owen *et al*., 2002a & b). Although growth rates in *B. undatum* are not constant throughout ontogeny (Hollyman *et al*., 2018a) they do vary seasonally. This annual variation in growth rate may be the cause of the largest offsets during temperature minima i.e. the period of slowest growth (Supplementary material Figure B) as growth rate varies with ambient seawater temperature.

4.5 Potential applications of newly calibrated equation

In practice, the methods outlined here could be applied to the management of this species through accurate age determination and reconstruction of historical seasonal growth rates. Whilst $\delta^{18}O_S$ has been used in previous studies to validate other age determination methods (opercula – Santarelli and Gros, 1986; statoliths – Hollyman *et al*., 2018c), it could be used in its own right as an ageing tool in the absence of opercula and statoliths (e.g. using discarded dead collected shells). Isotopic ageing methods have clear benefits over standard growth line counting techniques, although they are considerably more expensive. Not only can they be used to infer changes in sub-annual growth rate over time, but they can now be used to investigate the

environmental conditions (i.e. seawater temperature) present during periods of fast growth in this species. With increasing interest in the management of whelks and how biological parameters in *B. undatum* are influenced by seawater temperature (Emmerson *et al*., 2020), the methods outlined here could prove useful in informing the future management of this species.

These findings greatly increase the potential for reconstructing past environmental conditions from archaeological *B. undatum* shells. This species has been found in several shell Mesolithic and Neolithic shell-middens (Dupont 2006; Thomas and Mannino 1999). Specific examples of these findings include a midden on the Isle of White (UK) where their presence and condition have been used to infer the use of bottom fishing techniques in archaeological samples (i.e. dredging; Campbell and Russel, 2014) and also in St Andrews (Scotland) where they were used to suggest coastal foraging by historical inhabitants (Pearson, 1970). The use of $\delta^{18}O_s$ in sclerochronology of dead collected and archaeological shells often relies on the ability to cross match and absolutely date long-lived animals to infer long term trends in environmental conditions (Andrus, 2011; Reynolds *et al*., 2016). Whilst this is not possible for short-lived (<10 years) *B. undatum*, they do provide an excellent opportunity for reconstructing high resolution (daily and weekly) 'windows' of seawater temperature data due to their fast growth rates. 120 mm+ linear growth was often observed during 6-month fast growth periods (spring/summer); with a higher sampling resolution than the one used in this study, sub-weekly samples could easily be attained. Previous studies have also used short-lived mollusc species for reconstructions of palaeotemperatures and comparisons between modern and fossil specimens (e.g. *Aequipecten opercularis* [Johnson *et al*., 2009]; *Osilinus turbinatus* [Colonese *et al*., 2009]; Saxodomus gigantean [Hallman et al., 2009]). There is no reason, therefore, why similar studies could not be undertaken using *B. undatum* collected from shell middens as it would be possible to infer the season of collection from the $\delta^{18}O_s$ values of the most recently deposited shell material, providing information about ancient foraging trends (e.g. Mannino *et al*., 2003; Burchell *et al*., 2013). *B. undatum* shells have also been found during archaeological excavations in a gully near Rotterdam Harbour (Netherlands) with co-occurring material dated to either ~8000 or ~48,000 yr BP (Mol *et al*., 2006). Specimens such as these could now be used to reconstruct high-resolution windows of seawater temperature from before the last Glacial Maximum (~48,000 yr BP) and the early Holocene Boreal Period (~8000 yr BP).

5 Conclusions

This paper reports for the first time on the 4-layer structure and aragonite composition of *B. undatum* shells, assessed with micro-Raman spectroscopy. A species-specific palaeotemperature equation has been calculated from laboratory reared juvenile specimens, which enabled accurate high-resolution reconstructions of seawater temperature from the shells of wild caught specimens, something never before undertaken for this species. A clear offset between the equation presented here and previous equations is present and variable throughout the year. This annual variability in the offset suggests that a physiological process which changes on an annual time scale (such as growth rate) may be responsible. We have shown the accuracy of the $\delta^{18}O_s$ values in reconstructing seawater temperature using the newly calibrated equation. This highlights the potential of *B. undatum* shells as recorders of annual seawater temperature for both modern and historical specimens with potential applications in fisheries management and archaeology. The vital offset between the calibration presented here and previously published calibrations using molluscan aragonite remains an interesting area for future research. An investigation to see whether this is common to other (potentially fast-growing) gastropods or unique to *B. undatum* could be highly significant in understanding gastropod physiology and their evolutionary pathway, as well as being practically important for palaeotemperature reconstructions in other gastropod species of interest.

6 Acknowledgements

The authors thank the anonymous reviewers for their comments, which greatly improved the manuscript. This project was part of a Bangor University-CEFAS PhD scholarship awarded to PRH. Thanks to Gwyne Parry-Jones (School of Ocean Sciences, (SOS), Bangor University), Mark Hamilton (NAFC) and Jon Shrives (DoE Jersey) for their help with sample collection. Thanks also to Berwyn Roberts and all other colleagues in SOS who helped maintain juvenile whelks in the aquarium. MRS was undertaken following a successful rapid access request to the Diamond Light Source (SP13616-1). All stable isotope sampling was undertaken following a successful facility grant application to the NERC facility (now National Environmental Isotope Facility) Steering Committee (IP−1527−0515). We thank Carol Arrowsmith for isotope analysis of the water samples and Ben Marchant (BGS) for writing the MATLAB script used to create the average isotope profiles. Thanks to Dr Bee Berx (Marine Scotland), Peter Hughes (Bangor University), Olga Andres (CEFAS) and Jon Shrives (Department of the Environment, Jersey) for help obtaining water temperature data.

Data statement

All newly analysed isotopic data presented in this paper can be found in the associated excel file. The data used for comparison to previously published studies can be found within the associated references. Site water temperature data can be obtained from the following agencies, Shetland – Marine Scotland (oceanography@marlab.ac.uk), Jersey – Department of the Environment Jersey (environmentenquiries@gov.je). Water temperature data from the Menai Strait can be found within the associated excel file.

7 References

Andrus, C. F. T. (2011) Shell midden sclerochronology. *Quaternary Science Reviews*, 30, 2892–2905.

Arkhipkin, A., Bizikov, V., Doubleday, Z., Laptikhovsky, V.V., Lishchenko, F., Perales-Raya, C., Hollyman, P.R. (2018) Techniques for estimating the growth of molluscs. II: Cephalopods. Journal of Shellfish Research, 37(4), 783-792.

Behrensmeyer, A. K., and Turner, A. (2017) Taxonomic occurrences of Buccinum recorded in the Paleobiology Database. *Fossilworks*. http://fossilworks.org.

Bemis, B. E., Spero, H. J., and Thunell, R.C. (2002) Using species-specific paleotemperature equations with foraminifera: a case study in the Southern California Bight. *Marine Micropaleontology*, 46(3–4), 405–430.

Böhm, F., Joachimski, M. M., Dullo, W.C., Eisenhauer, A., Lehnert, H., Reitner, J., and Worheide, G. (2000) Oxygen isotope fractionation in marine aragonite of coralline sponges. Geochim Cosmochim Acta 64:1695–1703.

Bökenhans, V., Bigatti, G., and Averbuj, A. (2016) Age estimation methods in the marine gastropod *Buccinanops globulosus* comparing shell marks and opercula growth rings. *Marine Biology Research*, 12, 881-887.

Brinza, L., Schofield, P. F., Mosselmans, J. F. W., Donner, E., Lombi, E., Paterson, D., and Hodson, M. E. (2014) Can earthworm secreted calcium carbonate immobilise Zn in contaminated soils? *Soil Biology and Biochemistry*, 74, 1−10.

Burchell, M., Cannon, A., Hallmann, N., Schwarcz, H.P., and Schöne, B.R. (2013) Inter-site variability in the season of shellfish collection on the central coast of British Columbia. *Journal of Archaeological Science*, 40, 626-636. https://doi.org/10.1016/j.jas.2012.07.002

Campbell, G., and Russell, M. (2014) Direct Evidence for Bottom-fishing in Archaeological Whelks (*Buccinum undatum*). 'Human Exploitation of Aquatic Landscapes' special issue (Fernandes, R., and Meadows, J. eds.). *Internet Archaeology*. http://dx.doi.org/10.11141/ia.37.6

Colonese, A.C., Troelstra, S., Ziveri, P., Martini, F., Lo Vetro, D., and Tommasini, S. (2009) Mesolithic shellfish exploitation in SW Italy: seasonal evidence from the oxygen isotopic composition of *Osilinus turbinatus* shells. *Journal of Archaeological Science*, 36, 1935-1944. https://doi.org/10.1016/j.jas.2009.04.021

Craig, H. (1953) The geochemistry of the stable carbon isotopes. *Geochimica et Cosmochimica Acta*, 3, 53-92

Craig, H. (1957) Isotopic standards for carbon and oxygen and correction factors for mass-spectrometric analysis of carbon dioxide. *Geochimica et Cosmochimca Acta*, 12, 133-149.

Craig, H. (1965) The measurement of oxygen isotope palaeotemperatures, pp. In E. Tongiori (Eds.), *Stable Isotopes in Oceanographic Studies and Palaeotemperatures* (161-82). Pisa: Consiglio Nazionale delle Ricerche Laboratorio di Geologia Nucleare.

676 Dupont, C. (2006) La malacofaune de sites mésolithiques et néolithiques de la façade atlantique de la France:
677 contribution à l'économie et à l'identité culturelle des groupes concernés. *British Archaeological Reports*
678 *International Series* (1571). Oxford: Archaeopress.

679 Emmerson, J.A., Hollyman, P.R., Bloor, I.S.M., and Jenkins, S.R. (2020) Effect of temperature on the growth of
680 the commercially fished common whelk (*Buccinum undatum*, L.): A regional analysis within the Irish Sea.
681 *Fisheries Research*, 223, 105437.

682 Epstein, S., Buchsbaum, J. R., Lowenstam, H. A. and Urey, H. C. (1953) Revised carbonate-water isotopic
683 temperature scale. *Geological Society of America Bulletin*, 64, 1315-1326.

684 Fahy, E., Masterson, E., Swords, D., and Forrest, N. (2000) A second assessment of the whelk fishery *Buccinum*
685 *undatum* in the southwest Irish Sea with particular reference to its history of management by size limit. *Irish*
686 *Fisheries Investigations* 6.

687 Fenger, T., Surge, D., Schöne, B. and Milner, N. (2007) Sclerochronology and geochemical variation in limpet
688 shells (Patella vulgata): a new archive to reconstruct coastal sea surface temperature. *Geochemistry Geophysics*
689 *Geosystems* 8 (7), Q07001. http://dx.doi.org/ 10.1029/2006GC001488.

690 Flores, C., Gayo, E.M., Salazar, D. and Broitman, B.R. (2018) $\delta^{18}O$ of Fissurella maxima as a proxy for
691 reconstructing Early Holocene seasurface temperatures in the coastal Atacama desert (25°S) *Palaeogeography,*
692 *Palaeoclimatology, Palaeoecology*, 499, 22–34.

693 Food and Agriculture Organization species distribution maps.
694 http://www.fao.org/figis/geoserver/factsheets/species.html. Accessed 1/7/17

695 Ford, H.L., Schellenberg, S.A., Becker, B.J., Deutschman, D.L., Dyck, K.A. and Koch, P.L. (2010) Evaluating the
696 skeletal chemistry of Mytilus californianus as a temperature proxy: effects of microenvironment and ontogeny.
697 *Paleoceanography*, 25(1), PA1203. http://dx.doi.org/10.1029/2008PA001677.

698 Friedman, I., and O'Neil, J. R. (1977) Compilation of stable isotope fractionation factors of geochemical interest.
699 In M. Fleisher (Eds.) *Data of Geochemistry, 6th ed. U.S. Geological Survey Professional Paper*, 776, 1–37.

700 Friedman, I., O'Neil, J., and Cebula, G. (1982) Two new carbonate stable isotope standards. Geostandards
701 Newsletter, 61, 11-12.

702 Gentry, D. K., Sosdian, S., Grossman, E. L., Rosenthal, Y., Hicks, D., and Lear, C.H. (2008) Stable isotope and Sr/Ca
703 profiles from the marine gastropod *Conus ermineus*: testing a multiproxy approach for inferring
704 paleotemperature and Paleosalinity. *Palaios*, 23, 195-209.

705 Gillikin, D.P. (2005) Geochemistry of marine bivalve shells: the potential for paleoenvironmental
706 reconstructions. PhD Thesis, Vrije Universiteit Brussel, Belgium.

707 Goodwin, D.H., Gillikin, D.P., and Roopnarine, P.D. (2013) Preliminary evaluation of potential stable isotope
708 and trace element productivity proxies in the oyster *Crassostrea gigas. Palaeogeography Palaeoclimatology*
709 *Palaeoecology*, 373, 88–97.

710 Grossman, E. L., Ku, T. L. (1986) Oxygen and carbon isotope fractionation in biogenic aragonite – temperature
711 effects. *Chemical Geology*, 59, 59-74.

712 Hallmann, N., Burchell, M., Schöne, B.R., Irvine, G. V., and Maxwell, D. (2009) High-resolution
713 sclerochronological analysis of the bivalve mollusk *Saxidomus gigantea* from Alaska and British Columbia:
714 techniques for revealing environmental archives and archaeological seasonality *Journal of Archaeological*
715 *Science*, 36(10), 2353-2364. https://doi.org/10.1016/j.jas.2009.06.018

716 Hermoso, M., Chan, I. Z. X., McClelland, H. L. O., Heureux, A. M. C., and Rickaby, R. E. M. (2016) Vanishing
717 coccolith vital effects with alleviated carbon limitation. *Biogeosciences*, 13, 301-312.

718 Heude-Berthelin, C., Hégron-Macé, L., Legrand, V., Jouaux, A., Adeline, B., Mathieu, M., and Kellner, K. (2011)
719 Growth and reproduction of the common whelk *Buccinum undatum* in west Cotentin (Channel), France. *Aquatic*
720 *living resources*, 24, 317–327.

721 Hollyman, P. R. (2017) Age, growth and reproductive assessment of the whelk, *Buccinum undatum*, in coastal
722 shelf seas. PhD thesis, Bangor University. 404 pp.

723 Hollyman, P.R., Chenery, S.R.N., EIMF, Konstantin Ignatyev, Laptikhovsky, V.V. and Richardson, C.A (2019) Micro-
724 scale geochemical and crystallographic analysis of *Buccinum undatum* statoliths reveals annual periodicity of
725 visible growth rings. *Chemical Geology*, 526, 153-164.

726 Hollyman, P.R., Chenery, S.R.N., Leng, M.J., Laptikhovsky, V.V., Colvin, C. N. and Richardson, C.A. (2018a) Age
727 and growth rate estimations of the commercially fished gastropod *Buccinum undatum*. *ICES journal of marine*
728 *science*, 75(6), 2129-2144.

729 Hollyman, P.R., Laptikhovsky, V. V. and Richardson, C.A. (2018b) Techniques for estimating the growth of
730 molluscs. I: Gastropods. *Journal of Shellfish Research*, 37(4), 773-782.

731 Hollyman, P.R., Leng M.J., Chenery, S.R.N., Laptikhovsky, V.V. and Richardson, C.A (2018c) Statoliths of the whelk
732 *Buccinum undatum*: a novel age determination tool. *Marine Ecology Progress Series*, 598, 261-272

733 Johnson, A. L. A., Hickson, J. A., Bird, A., Schone, B. R., Balson, P. S., Heaton, T. H. E., and Williams, M. (2009)
734 Comparative sclerochronology of modern and mid-Pliocene (c. 3.5 Ma) *Aequipecten opercularis* (Mollusca,
735 Bivalvia): an insight into past and future climate change in the north-east Atlantic region. Palaeogeography
736 Palaeoclimatolagy Palaeoecology, 284, 164-179.

737 Kendall, C. and Caldwell, E.A. (1998) Chapter 2: Fundamentals of isotopegeochemistry. In: Kendall, C. and
738 MacDonnell, J.J. (Eds.),Isotope tracers in catchment hydrology. Elsevier Science B.V., Amsterdam, pp. 51–86.

739 Kim, S.-T., Hillaire-Marcel, C. and Mucci, A. (2006) Mechanisms of equilibrium and kinetic oxygen isotope
740 effects in synthetic aragonite at 25°C. *Geochimica et Cosmochimica Acta*, 70, A318.

741 Kim, S-T., and O'Neil, J. R. (1997) Equilibrium and nonequilibrium oxygen isotope effects in synthetic carbonates.
742 *Geochimica et Cosmochimica Acta*, 61, 3461–75.

743 Kim, S-T., Mucci, A., and Taylor, B. E. (2007) Phosphoric acid fractionation factors for calcite and aragonite
744 between 25 and 75°C: Revisited. *Chemical Geology*, 246, 135–146.

745 Kim, S.-T., Coplen, T. B., and Horita, J. (2015) Normalization of stable isotope data for carbonate minerals:
746 Implementation of IUPAC guidelines. *Geochimica et Cosmochimica Acta*, 158, 276-289.

747 Langer, G., Sadekov, A., Greaves, M., Nehrke, G., Probert, I., Misra, S., and Thoms, S. (2020) Li partitioning into
748 coccoliths of Emiliania huxleyi : evaluating the general role of "vital effects" in explaining element partitioning
749 in biogenic carbonates. Geochemistry, Geophysics, Geosystems, 21, e2020GC009129.
750 https://doi.org/10.1029/2020GC009129

751 Latal, C., Piller, W. E., Harzhauser, M. (2004) Palaeoenvironmental reconstructions by stable isotopes of Middle
752 Miocene gastropods of the Central Paratethys. *Palaeogeography Palaeoclimatology Palaeoecology*, 211, 157-
753 169.

754 Legendre, P. (2014). lmodel2: Model II Regression. R package version 1.7-2. https://CRAN.R-
755 project.org/package=lmodel2

756 Leng, M. J., and Lewis, J. P. (2016) Oxygen isotopes in Molluscan shell: Applications in environmental
757 archaeology. *Environmental Archaeology*, 21(3), 295-306.

758 Leng, M. J., and Marshall, J. D. (2004) Palaeoclimate interpretation of stable isotope data from lake sediment
759 archives. *Quaternary Science Reviews*, 23(7-8), 811-831.

760 Lutz, R. A., and Rhoads, D. C. (1977) Anaerobiosis and a Theory of Growth Line Formation. *Science*, 198(4323),
761 1222-1227.

762 Magnúsdóttir H, Pálsson S, Westfall KM, Jónsson ZO, Örnólfsdóttir EB (2019) Morphological variation in
763 genetically divergent populations of the common whelk, Buccinum undatum (Gastropoda: Buccinidae), across
764 the North Atlantic. Biol J Linn Soc 128:93–106.

765 Mannino, M. A., Spiro, B. F., and Thomas, K. D. (2003) Sampling shells for seasonality: oxygen isotope analysis
766 on shell carbonates of the inter-tidal gastropod *Monodonta lineata* (da Costa) from populations across its
767 modern range and from a Mesolithic site in southern Britain. *Journal of Archaeological Science*, 30, 667–79.

768 Marine Management Organisation (2019) UK Sea Fisheries Statistics 2018. Office for National Statistics, London.
769 174pp.

770 McConnaughey, T. (1989a) ^{13}C and ^{18}O isotopic disequilibrium in biological carbonates: I. Patterns. *Geochimica*
771 *et Cosmochimica Acta,* 53, 151-162.

772 McConnaughey, T. (1989b) ^{13}C and ^{18}O isotopic disequilibrium in biological carbonates: I. In vitro simulation of
773 kinetic isotope effects. *Geochimica et Cosmochimica Acta,* 53, 163-171.

774 Mckenna, C., Berx, B., and Austin, W.E.N. (2016) The decomposition of the Faroe-Shetland Channel water masses
775 using Parametric Optimum Multi-Parameter analysis. *Deep-Sea Research pt I*, 107, 9–21.

776 Mickler, P.J., Banner, J.L., Stern, L., Asmerom, Y., Edwards, R.L. and Ito,E. (2004) Stable isotope variations in
777 modern tropical speleothems: Evaluating equilibrium vs. kinetic isotope effects. *Geochimica et Cosmochimica*
778 *Acta*, 68, 4381–4393.

779 Owen, R., H. Kennedy, and C. Richardson (2002a) Isotopic partitioning between scallop shell calcite and
780 seawater: Effect of shell growth rate. *Geochimica et Cosmochimica Acta*, 66, 1727 – 1737, doi:10.1016/S0016-
781 7037(01)
782 00882-1.

783 Owen, R., Kennedy, H. A., and Richardson, C. A. (2002b) Experimental investigation into partitioning of stable
784 isotopes between scallop (*Pecten maximus*) shell calcite and sea water. *Palaeogeography Palaeoclimatology*
785 *Palaeoecology*, 185(1-2), 163-174.

786 Parker, J. E., Thompson, S. P., Lennie, A. R., Potter, J., and Tang, C. C. (2010) A study of the aragonite–calcite
787 transformation using Raman spectroscopy, synchrotron powder diffraction and scanning electron microscopy.
788 *CrystEngComm*, 12, 1590–1599. doi: 10.1039/b921487a

789 Patterson, W., Smith, G. and Lohmann, K. (1993) Continental paleo thermometry and seasonality using the
790 isotopic composition of aragonite otoliths of freshwater fishes. *Geophysical Monographs*, 27, 199–202.

791 Pearson, R. (1970). Archaeological Investigations in the St. Andrews Area, New Brunswick. *Anthropologica, 12*(2),
792 181-190. doi:10.2307/25604826

793 Prendergast, A. L., Azzopardi, M., O'Connell, T. C., Hunt, C., Barker, G., and Stevens, R. E. (2013) Oxygen isotopes
794 from *Phorcus* (*Osilinus*) *turbinatus* shells as a proxy for sea surface temperature in the central Mediterranean: A
795 case study from Malta. *Chemical Geology*, 354, 77-86.

796 Prendergast, A. L., Stevens, R. E., Barker, G., and O'Connell, T. C. (2015) Oxygen isotope signatures from land
797 snail (*Helix melanostoma*) shells and body fluid: Proxies for reconstructing Mediterranean and North African
798 rainfall. *Chemical Geology*, 409, 87–98.

799 Prendergast, A.L. and Schöne, B.R. (2017) Oxygen isotopes from limpet shells: implications for
800 palaeothermometry and seasonal shellfish foraging studies in the Mediterranean. *Palaeogeography*
801 *Palaeoclimatolagy Palaeoecology*. 484, 33–47.

R Core Team (2019). R: A language and environment for statistical computing. R Foundation for Statistical Computing, Vienna, Austria. URL: https://www.R-project.org/.

Radtke, R.L., Showers, W., Moksness, E. and Lenz, P. (1998) Environmental information stored in otoliths: insights from stable isotopes. *Marine Biology*, 132(2), 347-348.

Reynolds, D. J., Richardson, C. A., Scourse, J. D., Butler, P. G., Wanamaker, A. D., Ridgway, I., Sayer, M. D. J., and Gulliver, P. (2013) The potential of the marine bivalve mollusc *Glossus humanus* (L.) as a sclerochronological archive. *The Holocene*, 23(12), 1711– 1720.

Reynolds, D. J., Scourse, J. D., Halloran, P. R., Nederbragt, A. J., Wanamaker, A. D., Butler, P. G., Richardson, C. A., Heinemeier, J., Eiríksson, J., Knudsen, K. L., and Hall, I. R. (2016) Annually resolved North Atlantic marine climate over the last millennium. *Nature Communications*, 7, 13502.

Richardson, C. A. (2001) Molluscs as archives of environmental change. *Oceanography and Marine Biology, An Annual Review*, 39, 103–164.

Santarelli, L., and Gros, P. (1985) Age and growth of the whelk *Buccinum undatum* L. (Gastropoda: Prosobranchia) using stable isotopes of the shell and operculum striae. *Oceanologica Acta*, 8(2), 221–229.

Schöne, B. R., Houk, S. D., Castro, A. D. F., Fiebig, J., Oschmann, R., Krönke, I., and Dreyer, W., Gosselck, F. (2005) Daily Growth Rates in Shells of *Arctica islandica*: Assessing Sub-seasonal Environmental Controls on a Long-lived Bivalve Mollusk. *Palaios*, 20(1), 78-92.

Schöne, B. R., Rodland, D. L., Wehrmann, A., Heidel, B., Oschmann, W., Zhang, Z., Fiebig, J., and Beck, L. (2007) Combined sclerochronologic and oxygen isotope analysis of gastropod shells (*Gibbula cineraria*, North Sea): life-history traits and utility as a high-resolution environmental archive for kelp forests. *Marine Biology*, 150(6), 1237-1252.

Schwarz, R., Hoving, H-J., Noever, C. and Piatkowski, U. (2019) Life histories of Antarctic incirrate octopods (Cephalopoda: Octopoda). *PLoS ONE*, 14(7), e0219694. https://doi.org/10.1371/journal.pone.0219694

Sharma, T., and Clayton, R. N. (1965) Measurement of 18O/16O ratios of total oxygen of carbonates. *Geochimica et Cosmochimica Acta*, 56, 419–430.

Sosdian, S., Gentry, D. K., Lear, C. H., Grossman, E. L., Hicks, D., and Rosenthal, Y. (2006) Strontium to calcium ratios in the marine gastropod *Conus ermineus*: growth rate effects and temperature calibration. *Geochemistry Geophysics Geosystems*, 7(11), 1525-2027.

Spero, H.J., Bijma, J., Lea, D.W., and Bemis, B.E. (1997) Effect of seawater carbonate concentration on foraminiferal carbon and oxygen isotopes. *Nature*, 390, 497–500.

Steinheart, J., Butler, P. G., Carroll, M. L., and Hartley, J. (2016) The application of long-lived bivalve sclerochronology in environmental baseline monitoring. *Frontiers in Marine Science*, 3, 176. doi: 10.3389/fmars.2016.00176

Thébault, J., L. Chauvaud, J. Clavier, J. Guarini, R. B. Dunbar, R. Fichez, D. A. Mucciarone and E. Morize (2007) Reconstruction of seasonal temperature variability in the tropical Pacific Ocean from the shell of the scallop, *Comptopallium radula*. *Geochimica et Cosmochimica Acta*, 71, 918 – 928, doi:10.1016/j.gca.2006. 10.017.

Thomas, K. and Mannino, M. (1999) The bioarchaeology of the Culverwell shell midden'. In S. Palmer (Eds.) Culverwell Mesolithic Habitation Site (Isle of Portland, Dorset): Excavation Report and Research Studies. *British Archaeological Reports* (287, 94-106). Oxford: Archaeopress.

Urey, H.C., Lowenstam, H.A., Epstein, S., and McKinney, C.R. (1951) Measurement of paleotemperatures and temperatures of the Upper Cretaceous of England, Denmark, and the southeastern United States. *Geological Society of America Bulletin*, 62, 399-416.

845 Vasconcelos, P., Gharsallah, I. H., Moura, P., Zamouri-Langar, L., Gaamour, A., and Missaoui, H. (2012) Appraisal
846 of the usefulness of operculum growth marks for ageing *Hexaplex trunculus* (Gastropoda: Muricidae):
847 Comparison between surface striae and adventitious layers. *Marine Biology Research*, 8, 141-53.

848 Vitale, F.,Worsøe Clausen,L., and NíChonchúir, G.(Eds.) (2019) Handbook of fish age estimation protocols and
849 validation methods. ICES Cooperative Research Report No.346.180pp. http://doi.org/10.17895/ices.pub.5221

850 Wanamaker, A. D., Kreutz, K. J., Borns, H. W., Introne, D. S., Feindel, S., and Barber, B. J. (2006) An aquaculture-
851 based method for calibrated bivalve isotope paleothermometry. *Geochemistry Geophysics Geosystems*, 7,
852 Q09011. doi:10.1029/2005GC001189.

853 Weetman, D., Hauser, L., Bayes, M.K., Ellis, J.R. and Shaw, P.W. (2006) Genetic population structure across a
854 range of geographic scales in the commercially exploited marine gastropod *Buccinum undatum*. *Marine*
855 *Ecology Progress Series*, 317, 157–169.

856 Wehrmeister, U., Jacob, D. E., Soldati, A. L., Loges, N., Häger, T., and Hofmeister, W. (2010b) Amorphous,
857 nanocrystalline and crystalline calcium carbonates in biological materials. *Journal of Raman Spectroscopy*, 42,
858 926–935.

859 Wehrmeister, U., Soldati, A. L., Jacob, D. E., Häger, T., and Hofmeister, W. (2010a) Raman spectroscopy of
860 synthetic, geological and biological vaterite: a Raman spectroscopic study. *Journal of Raman Spectroscopy*, 41,
861 193–201.

862 Weiner, S. and Dove; P.M. (2003) An Overview of Biomineralization Processes and the Problem of the Vital
863 Effect. *Reviews in Mineralogy and Geochemistry*, 54 (1), 1–29.

864 Wejnert, K. E., Thunell, R. C., and Astor, Y. (2013) Comparison of species-specific oxygen isotope
865 paleotemperature equations: Sensitivity analysis using planktonic foraminifera from the Cariaco Basin,
866 Venezuela. *Marine Micropaleontology*, 101, 76–88.

867 Wilbur, K.M. and Saleuddin, A.S.M. (1983) Shell formation. In: Saleuddin, A.S.M. and Wilbur, K.M. (Eds.),The
868 Mollusca—Volume 4: Physiology—Part 1. Academic Press, New York, pp. 235–287.

869 Zeebe, R.E. (1999) An explanation of the effect of seawater carbonate concentration on foraminiferal oxygen
870 isotopes. *Geochimica et Cosmochimica Acta*, 63, 2001–2007.

871 Ziveri, P., Stoll, H., Probert, I., Klaas, C., Geisen, M., Ganssen, G. and Young, J. (2003) Stable isotope “vital effects”
872 in coccolith calcite. *Earth and Planetary Science Letters*, 210, 137-149.

Electronic Appendix

Table A. Results of correlation analyses between $\delta^{13}C$ and $\delta^{18}O$ for individual shells. Significant results are displayed in bold.

Shell	Sex	Correlation	p	t	df	R^2	Adjusted R^2
Jersey - 1	M	0.123	0.236	1.194	93	0.015	0.004
Jersey - 2	M	0.125	0.227	1.217	93	0.016	0.005
Jersey - 3	M	0.101	0.32	1	97	0.01	0
Menai Strait - 1	F	**-0.337**	**0**	-4.276	143	0.113	0.107
Menai Strait - 2	M	-0.003	0.975	-0.031	100	0	-0.01
Menai Strait - 3	F	0.063	0.544	0.609	93	0.004	-0.007
Menai Strait - 4	M	-0.04	0.707	-0.377	91	0.002	-0.009
Menai Strait - 5	F	-0.033	0.74	-0.333	102	0.001	-0.009
Menai Strait - 6	M	**0.393**	**0**	4.38	105	0.154	0.146
Shetland - 1	M	**0.23**	**0.024**	2.3	95	0.053	0.043
Shetland - 2	M	**0.395**	**0**	4.428	106	0.156	0.148
Shetland - 3	M	**0.32**	**0.001**	3.542	110	0.102	0.094
Tank Grown - 1	M	**0.5**	**0**	4.588	63	0.25	0.239
Tank Grown - 2	M	**0.288**	**0.021**	2.366	62	0.083	0.068
Tank Grown - 3	M	**0.484**	**0**	4.138	56	0.234	0.221

Table B, Outputs (p & F values) from ANCOVA analyses following regression of chosen published palaeotemperature equations against the calibrated *B. undatum* data.

	Slope		Intercept	
Study	f-ratio	p value	f-ratio	p value
Grossman & Ku, 1986 (mollusc aragonite)	1.18	0.283	474.97	**<0.0001**
Grossman & Ku, 1986 (total, mollusc & foram aragonite)	4.31	**0.040**	193.48	**<0.0001**
Kim *et al*., 2007 (abiogenic aragonite)	0.12	0.729	492.87	**<0.0001**
Epstein *et al*., 1953 (mix of biogenic aragonite & calcite)	8.12	**0.006**	8.33	**0.005**
Kim & O'Neil, 1997 (abiogenic calcite)	1.57	0.216	86.99	**<0.0001**

Table C. A comparison of the average reconstructed seawater temperature deviation from the recorded seawater temperature over the period of growth during the *Buccinum undatum* calibration with relevant equations taken from the literature (± 1SE). The % of the observed SST range reconstructed by each equation is also shown.

Equation	Calibration material	Average deviation from temperature (°C)	SD	SE	% of observed temperature range reconstructed
1. Grossman & Ku, 1986	mollusc aragonite	-6.22	1.99	0.05	36.37
2. Grossman & Ku, 1986	mollusc & foram aragonite	-3.46	2.05	0.05	53.18
3. Kim et al., 2007	abiogenic aragonite	-4.90	1.94	0.05	47.28
4. Epstein et al., 1953	mix of biogenic aragonite & calcite	-1.46	2.03	0.05	69.35
5. Kim & O'Neil, 1997	abiogenic calcite	-1.53	1.94	0.05	69.94
6. This Study	mollusc aragonite	0.11	1.93	0.05	78.79

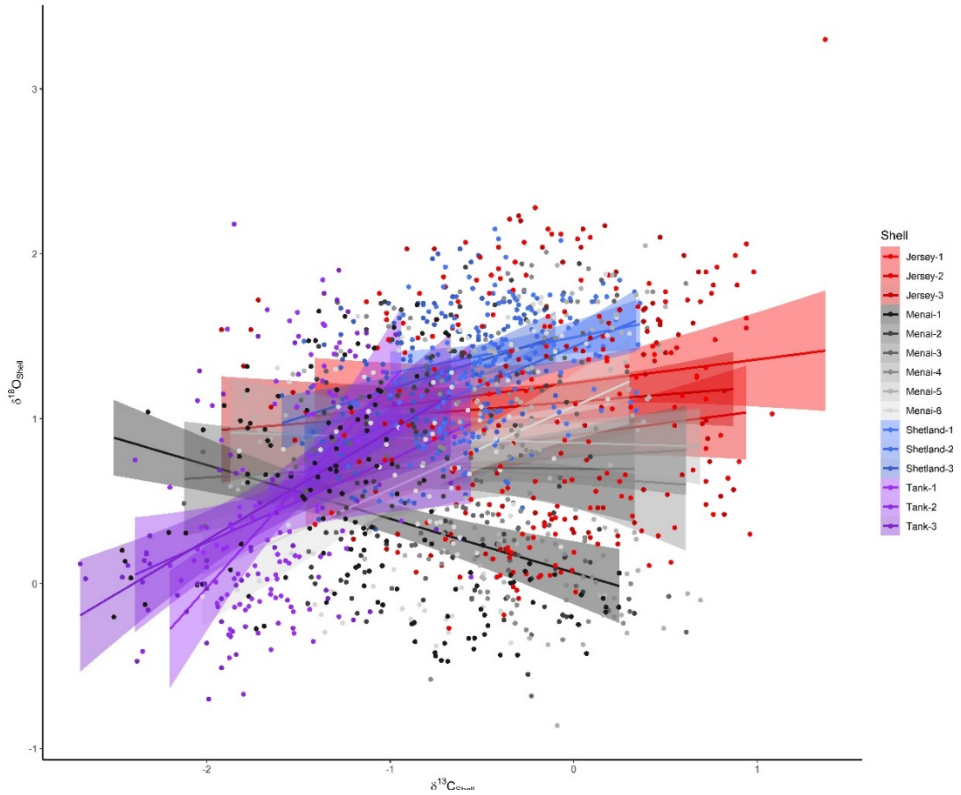

Figure A. $\delta^{13}C$ plotted against $\delta^{18}O$ for all measured shells. Linear fits have been plotted, shaded areas represent 95% CI.